Nano Research 2018, 11(7): 3519–3528
https://doi.org/10.1007/s12274-017-1793-y
Research Article
ISSN 1998-0124
CN 11-5974/O4

Ultra-dense planar metallic nanowire arrays with extremely large anisotropic optical and magnetic properties

Qi Jia[1,2,4], Xin Ou[1,2] (✉), Manuel Langer[1], Benjamin Schreiber[1], Jörg Grenzer[1], Pablo F. Siles[3], Raul D. Rodriguez[3,5], Kai Huang[1,2,4], Ye Yuan[1], Alireza Heidarian[1], René Hübner[1], Tiangui You[2], Wenjie Yu[2], Kilian Lenz[1], Jürgen Lindner[1], Xi Wang[2], and Stefan Facsko[1]

[1] *Helmholtz-Zentrum Dresden-Rossendorf, Institute of Ion Beam Physics and Materials Research, Bautzner Landstr. 400, 01328 Dresden, Germany*
[2] *State Key Laboratory of Functional Material for Informatics, Shanghai Institute of Microsystem and Information Technology, Chinese Academy of Sciences, Shanghai 200050, China*
[3] *Technische Universität Chemnitz, Reichenhainerstraße 70, 09107 Chemnitz, Germany*
[4] *University of Chinese Academy of Sciences, Beijing 100049, China*
[5] *Tomsk Polytechnic University, 30 Lenin Ave., 634050 Tomsk, Russia*

Received: 18 May 2017
Revised: 4 August 2017
Accepted: 6 August 2017

KEYWORDS

self-assembly,
metallic nanowire array,
reverse epitaxy,
magnetic anisotropy,
anisotropic dielectric function

ABSTRACT

A nanofabrication method for the production of ultra-dense planar metallic nanowire arrays scalable to wafer-size is presented. The method is based on an efficient template deposition process to grow diverse metallic nanowire arrays with extreme regularity in only two steps. First, III-V semiconductor substrates are irradiated by a low-energy ion beam at an elevated temperature, forming a highly ordered nanogroove pattern by a "reverse epitaxy" process due to self-assembly of surface vacancies. Second, diverse metallic nanowire arrays (Au, Fe, Ni, Co, FeAl alloy) are fabricated on these III-V templates by deposition at a glancing incidence angle. This method allows for the fabrication of metallic nanowire arrays with periodicities down to 45 nm scaled up to wafer-size fabrication. As typical noble and magnetic metals, the Au and Fe nanowire arrays produced here exhibited large anisotropic optical and magnetic properties, respectively. The excitation of localized surface plasmon resonances (LSPRs) of the Au nanowire arrays resulted in a high electric field enhancement, which was used to detect phthalocyanine (CoPc) in surface-enhanced Raman scattering (SERS). Furthermore, the Fe nanowire arrays showed a very high in-plane magnetic anisotropy of approximately 412 mT, which may be the largest in-plane magnetic anisotropy field yet reported that is solely induced via shape anisotropy within the plane of a thin film.

Address correspondence to ouxin@mail.sim.ac.cn

1 Introduction

Because of their large surface-to-volume ratio with very high shape anisotropy [1], ultra-dense nanostructured metal arrays could be integrated into high-density memory devices [2], interconnections in integrated circuits [3], plasmonic devices [4], nanoelectrodes [5], thermal heaters [6], and biological nano-sensors [7], applications that have attracted much attention in recent years. Conventionally, metallic nanowires are fabricated by top-down approaches, e.g., optical lithography, which makes it possible to fabricate planar nanowire (NW) arrays. However, the spatial resolution of such arrays is constrained by the optical diffraction limit, making nanoscale application unattainable [8]. Although electron-beam lithography offers a high patterning quality at a much better dimensional limit, the fabrication of nanowire arrays in a periodicity regime below 50 nm is still very challenging. Moreover, electron-beam lithography is quite inefficient for patterning at the wafer-scale level.

In contrast to top-down approaches, nanofabrication techniques based on self-organization and self-assembly allow for simple and low-cost production of dense metallic nanowire arrays, and thus such techniques have been considered as promising complementary methods [9, 10]. One method, which only allows the fabrication of vertical nanowire arrays, is electrodeposition via nanoporous templates such as anodized aluminum oxide films with a high density of nanopores [11–13]. However, there is a broad size distribution, and it is difficult to place the nanowires at a specific location for device fabrication and investigation. Another effective approach to fabricating planar metallic nanowire arrays is using glancing-angle deposition on a self-organized nanopatterned substrates [14]. Because of the self-masking effects, the periodicity and the regularity of the metallic nanowires depend significantly on the surface structure of the templates. The quality of the templates is a key issue to fabricating the metallic nanowire arrays. The faceted surfaces can be achieved by several techniques, such as thermal etching (NaCl [15]), semiconductor heteroepitaxy (GeSi-on-Si [16]), and high-temperature annealing (sapphire [17]). These nanopatterned surfaces have been applied as templates to fabricate metallic nanostructure arrays by shadow deposition [18–20]. However, the numerous topographic defects and relatively large periodicity of these templates still limit the practical application of metallic nanowire arrays. Self-organized surface patterns on semiconductors and oxide surfaces can be also induced by low-energy ion irradiation [21, 22]. For example, self-organized nanoscale wave structures on Si surfaces were produced by low-energy ion beam irradiation at room temperature [23–26]. Such wave structures can serve as templates for the fabrication of low-dimensional metallic nanostructure arrays, and the periodicity size can be reduced to below 50 nm [27–29]. Still, the main drawback of this method is that the Si surface is amorphized during ion bombardment at room temperature [30], and the presence of numerous topographic defects in the amorphous surface pattern is a serious disadvantage for the application of these patterns as templates for regular metallic nanowire arrays.

Previously, we reported that faceted and crystalline nanopatterns can be fabricated via a so-called "reverse epitaxy" process on different semiconductor surfaces [31]. Above the recrystallization temperature of the materials, ion irradiation can be employed to produce highly ordered and crystalline patterns consisting of specific crystalline facets depending on the crystal structure and the surface orientation. These patterns are self-aligned, with a high degree of ordering along a specific crystal orientation. On single crystalline III-V surfaces with zinc-blende structures, e.g. GaAs (001) and InAs (001), the periodic nanogrooves are oriented along the $[1\bar{1}0]$ direction [32, 33]. Here, we demonstrate that these ordered patterns can potentially serve as templates for the fabrication of diverse metallic nanowire arrays (Au, Fe, Ni, Co, and FeAl alloy) consisting of well-separated nanowires with a periodicity below 50 nm. As a typical example, noble (Au) and magnetic (Fe) metal nanowire arrays were produced, which exhibited extremely large anisotropic optical and magnetic properties, respectively. In addition, the patterns of the crystalline GaAs surfaces could provide a platform for growing epitaxial Fe nanowires, which could be used as build blocks for the development of spintronics based on an Fe/GaAs system [34, 35].

2 Experimental section

2.1 Preparation of the patterned template

The ordered nanogroove patterns were formed on epi-ready GaAs (001) and InAs (001) by normal incidence of 1 keV Ar^+ irradiation at 410 °C for GaAs (100) and 350 °C for InAs (100), respectively. An ion fluence of 1×10^{19} cm^{-2} was applied during the irradiation process.

2.2 Fabrication of metallic nanowire arrays

Au, Fe, Ni, Co, and FeAl alloy nanowires with thicknesses of 20 nm were deposited by molecular beam epitaxy (MBE). The metal deposition process was performed on the faceted GaAs (001) surface with a glancing angle of 80° to the surface normal (shadow deposition). The metallic nanowire arrays were formed on the facets of the nanogrooves. To avoid oxidization of the Fe nanowires, a 10-nm-thick Rh layer was deposited as a capping layer on the Fe in two steps, with incidence angles of 80° and 45°, respectively.

2.3 Grazing incidence small-angle X-ray scattering measurements

Grazing incidence small-angle X-ray scattering (GISAXS) measurements were performed on a modified Empyrean diffractometer equipped with two-dimensional side-by-side optics and an extended fine-focus Cu tube with a point spot size of 150 μm. We used a pixel detector (516 × 516 pixels, with a 55 μm pixel size) to register the scattering signal. This setup allowed us to work without any beam stop. The sample–detector distance was set to 500 mm. The incident angle was set to 0.42° for all cases.

2.4 Electrical characterization

Atomic force microscopy (AFM) measurements for the Au nanowire arrays were performed using an Agilent 5500 AFM system to investigate the topography and the electrical characterization characteristics via Kelvin force microscopy (KFM). The measurements were performed under a well-controlled N_2 environment to preserve the integrity and avoid possible contamination of the samples, as well as to circumvent the possible influence of the ambient conditions on the electrical measurements. Silicon probes with an electrically conductive coating (Cr/Pt), typical force constant of 3 $N \cdot m^{-1}$ and resonance frequency of 75 kHz, were employed for simultaneous topography and electrical measurements. This enables a direct correlation between the topography and the electric characteristics of the samples. Measurements were performed in tapping mode ensuring minimal contact between the AFM probe and the sample surface with a very high resolution. For KFM measurements, a feedback loop allows for maintaining a DC probe bias that counteracts the surface electrostatic force. This enables a quantitative analysis of changes of the electric charge distribution along across the sample surface.

2.5 Optical characterization

Ellipsometry measurements were performed with a Woollam M-2000FI. A 2-nm-thick CoPc thin layer was deposited in vacuum at 10^{-10} mbar controlled by a quartz crystal microbalance detector. For the Raman spectroscopy measurement, a LabRam HR800 spectrometer was used in backscattering geometry with a 50× long working distance objective (N.A. = 0.5). The Raman signal was decomposed by a 600 lines/mm grating and recorded with an electron-multiplying charge-coupled device (CCD) detector. The laser power was set to 1 mW.

2.6 Magnetic characterization

The magnetic characterization was carried out using a broadband ferromagnetic resonance (FMR) setup with tunable frequencies from 10 MHz to 50 GHz. The magnetic system was excited by a microwave field generated by an Agilent E8364B vector network analyzer, which was coupled into a coplanar waveguide where the sample is mounted flip-chip. The complex transmission parameter S_{21} was recorded as the FMR signal during a field sweep at a constant frequency.

3 Results and discussion

The fabrication process of metallic nanowire arrays is illustrated schematically in Fig. 1. The process consists of only two steps: (1) The III-V crystalline semicon-

ductor surfaces are pre-patterned by low-energy ion irradiation at an elevated temperature above the recrystallization temperature of the materials (Fig. 1(a)); (2) the metal is deposited on the periodically patterned surface at a glancing incidence angle, which is typically 60°–80° to the surface normal and perpendicular to the nanogroove axis (Fig. 1(b)). In the first step, the normal incidence ion irradiation of III-V surfaces at an elevated temperature leads to periodic faceted grooves oriented along the [1$\bar{1}$0] direction with a remarkably high order, as shown in Fig. 1(c). The Fourier transform in the inset shows well-resolved high order interferences, which indicate the lateral ordering of the faceted nanostructure. The surface instability, which is responsible for the formation of these structures, results from the restrictions in the surface diffusion of vacancies due to the Ehrlich–Schwoebel barrier at the step-edges [36]. For III-V semiconductors with a zinc-blende structure, the [1$\bar{1}$0]- and [110]-aligned step-edges are no longer energetically equal. A symmetry-breaking driving force exists on the (001) surfaces of these materials due to the stacking of alternating planes of Ga(In)As and to the exclusive formation of dimer rows of Ga (In). The facets observed on the ion-irradiated surfaces are close to the {114} crystal planes, which have an angle of 19.47° with the GaAs (001) and the InAs (001) surfaces (see Fig. S1 in the Electronic Supplementary Material (ESM)). The periodicity and facet orientation can be tuned by using a surface with different miscuts or by applying different irradiation conditions [32]. In the second step, because of the self-shadowing effect, the metal was deposited on the sidewalls of the facets facing the deposition beam instead of on the bottom of the nanogrooves; thus, ordered metallic nanowire arrays were formed with the same periodicity as the nanogrooves (Fig. 1(d)). Therefore, the periodicity of the metallic nanowire arrays can be tuned by using templates with different periodicities (typically in the 45–100 nm range). In addition, the size of the nanowires can be altered by varying the deposition thickness of the metal (see Fig. S2 in the ESM).

In this study, different metallic nanowire arrays were successfully deposited on the faceted GaAs (001) surfaces. Figures 2(a) and 2(b) show the top views of the scanning electron microscopy (SEM) of Au and

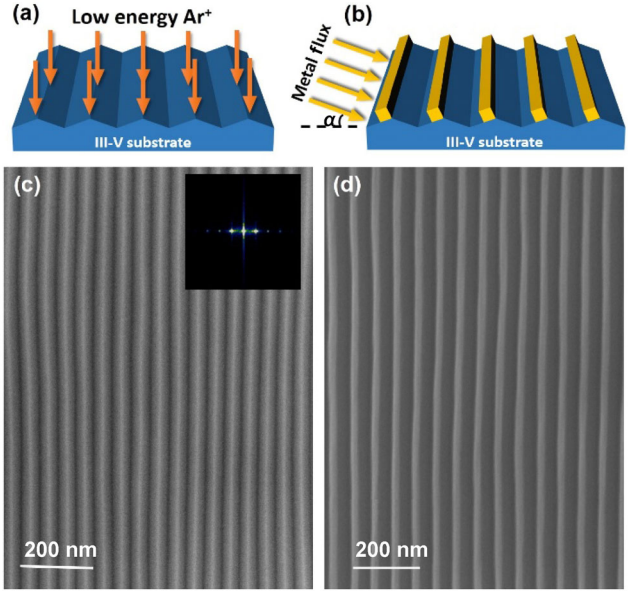

Figure 1 Schematic illustration and SEM top-down images of the ordered and faceted nanogroove pattern preparation and the metallic nanowire array formation: (a) and (c) The faceted nanogroove array is formed on III-V surfaces in only one step under low-energy Ar^+ irradiation. (b) and (d) Metallic nanowires on III-V facets are fabricated by deposition under a glancing incidence angle. The inset of (c) is the fast Fourier transform (FFT) pattern of the SEM image.

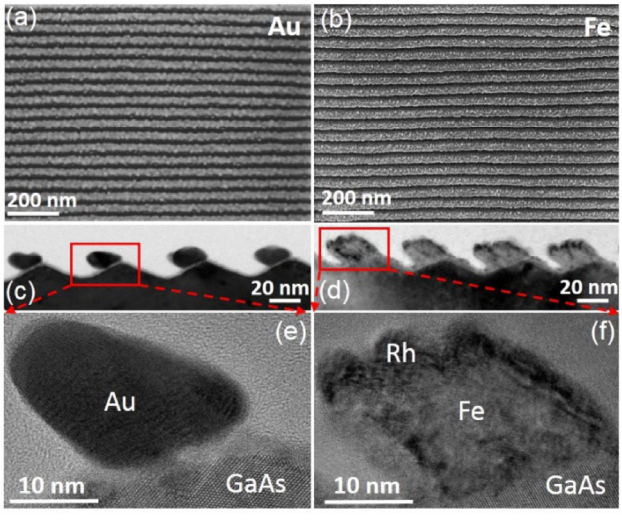

Figure 2 Top-down SEM and cross-sectional transmission electron microscopy (TEM) of highly ordered Au and Fe nanowire arrays deposited on faceted GaAs (100) surfaces. (a) and (b) SEM images of Au and Fe nanowire arrays. (c) and (d) Cross-sectional bright-field TEM images of the Au and Fe nanowires, and (e) and (f) the corresponding high-resolution TEM images. To avoid oxidization of the Fe nanowires, 10 nm of Rh was deposited as a capping layer.

Fe nanowires deposited on the faceted GaAs surfaces by MBE. Ni, Co, and FeAl alloy nanowire arrays were also produced by this method, as shown in Fig. S3 in the ESM. The deposition thickness of the metal was approximately 20 nm, with the metallic nanowire arrays all aligned along the [1$\bar{1}$0] direction. To avoid oxidization of the Fe nanowires, a 10-nm-thick layer of Rh was deposited as a capping layer. To see the morphology of the metallic nanowire arrays on a smaller scale, cross-sectional transmission electron microscopy (XTEM) was performed, as shown in Figs. 2(c) and 2(d). It was found that the metallic nanowires were located on the side of the facets exposed to the deposition beam. The periodicity of the metallic nanowire arrays was approximately 45 nm, with an inter-nanowire spacing of less than 20 nm. These dimensions reveal the remarkably high integration density of the metallic nanowires. In addition, the morphology of the metallic nanowire arrays can be improved by annealing in high vacuum. The surface became smoother after annealing at 250 °C (see Fig. S4 in the ESM). As indicated by Figs. 2(e) and 2(f), the Au and Fe nanowires were mainly polycrystalline. This may have been the result of native oxide layer formation on the crystalline GaAs facets as the sample was taken out of the irradiation chamber. To achieve the growth of epitaxial Fe nanowires on the crystalline GaAs facets, careful surface treatment is needed to remove the native oxide layer [37, 38].

In addition to SEM and XTEM measurements, GISAXS analysis makes it possible to measure the lateral ordering and orientation of the metallic nanowire arrays in macroscopic length scales [39, 40]. Figure 3(a) shows the GISAXS patterns of the Fe nanowire arrays measured just above the critical angle of total external reflection [41], as demonstrated in Fig. 2(b). The asymmetry of the intensity distribution resulted from the fact that the Fe nanowires were deposited on one side of the faceted substrates [42]. Compared with the GISAXS results shown in Ref. [42], the GISAXS patterns in our work are well separated

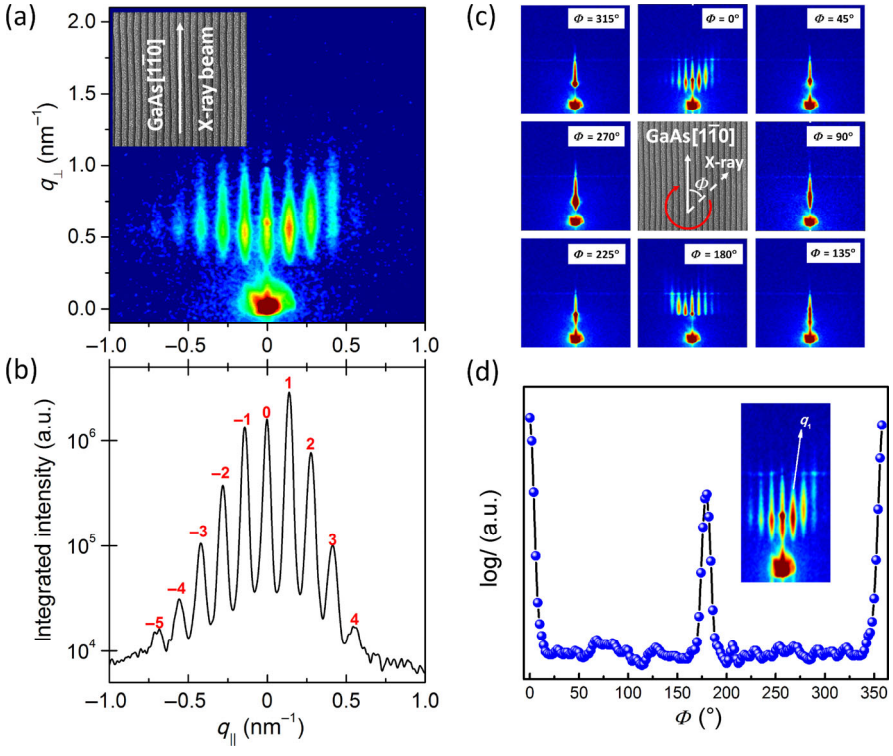

Figure 3 GISAXS pattern of Fe nanowire arrays on the faceted GaAs substrate. The X-ray beam followed the direction of GaAs [1$\bar{1}$0], and the incident angle was set to be 0.42°. The line profiles of (a) as a function of the scattering vector is shown in (b). $\boldsymbol{q}_{||}$ is the in-plane scattering vector. (c) The X-ray beam followed the GaAs [1$\bar{1}$0] direction ($\Phi = 0°$), and the sample stage was rotated to 45°, 90°, 135°, 180°, 225°, 270°, and 315°. (d) Plot of the intensities of the first-order diffraction peak q_1 (the white arrow) as a function of rotation angle.

and more distinct. In addition, the grating rods of the GISAXS patterns changed sharply as a function of rotation angle Φ (Figs. 3(c) and 3(d)). This indicates that the Fe nanowire arrays fabricated here were well ordered and oriented along a single direction over macroscopic length scales. Figure 3(b) shows an integrated line profile over the entire grating signal along the in-plane scattering vector ($q_{\parallel}$). The periodicity of the nanowire was calculated to be 45 nm, which is in agreement with the value obtained from Fig. 2(d).

Noble metal nanostructures generally exhibit unique optical properties in the visible spectral range because of the excitation of localized surface plasmon resonances (LSPRs) [27, 43, 44], which generates many appealing phenomena such as surface-enhanced Raman spectroscopy (SERS) [45–47]. In this work, the Au nanowire arrays were characterized optically by spectroscopic ellipsometry and Raman spectroscopy. As shown in Fig. 4(a), polarization-dependent results of the effective dielectric function show a significant optical anisotropy response depending on the electric field orientation with respect to the nanowire axis. The polarization of the incident light was chosen to be parallel ($E_{\parallel}$) or perpendicular ($E_{\perp}$) to the nanowires. The imaginary part of the effective dielectric function, Imag[ε_{eff}], reveals the optical properties of the fabricated nanostructures, and in particular the wavelength range where the plasmonic excitations occur (absorption). From the black line shown in Fig. 4(a), the peak at 270 nm, the double peaks at 400 and 420 nm, and the step at 875 nm are related to the band structure of the GaAs substrate. After the deposition of 30-nm-thick Au nanowires, the dominance of the GaAs peaks vanishes. Different behaviors in Imag[ε_{eff}] can be observed for $E_{\parallel}$ and $E_{\perp}$. For the case of $E_{\parallel}$, Imag[ε_{eff}] increases with the increasing wavelength, which suggests typical Drude behavior of continuous metallic films [48]. In contrast, Drude-type behavior is absent in $E_{\perp}$; instead, a dominant absorption peak at approximately 600 nm appears, as shown by the blue dashed line in Fig. 5(a), which comes from the LSPRs. Here, we observe a clearly resolvable LSPR peak in Imag[ε_{eff}] for $E_{\perp}$, which confirms the results above regarding the well-defined shape and separation of the Au nanowires. The excitation of localized surface plasmons results in a high electric field enhancement, which is frequently used in high-sensitivity molecular detection in SERS. For example, ultrathin films of phthalocyanine (CoPc) are usually challenging to detect by Raman spectroscopy because of the inefficient nature of inelastic scattering during the measurements [49]. However, plasmonic enhancement from metallic nanowires helps overcome this sensitivity limitation, as discussed below. The black line in Fig. 4(b) suggests that the feature Raman peaks of a 2-nm-thick CoPc layer cannot be well observed on a bare GaAs substrate. Regardless of the faintly resolved peaks, a plateau appears between 850 and 1,000 cm^{-1} that belongs to the GaAs substrate. In contrast, a clearly resolved Raman spectrum of CoPc was measured on the plasmonic Au nanowires, as indicated by the red line in Fig. 4(b), because the wavelength of the HeNe laser used during the measurement (633 nm wavelength, 1 mW) matched the LSPR of the Au nanowires. The SERS enhancement factor at the peak of 1,540 cm^{-1} can be estimated as ~ 130. It is concluded that this self-aligned Au nanowire array is an efficient substrate for SERS applications. In addition, noble metal nanowires are ideal candidates

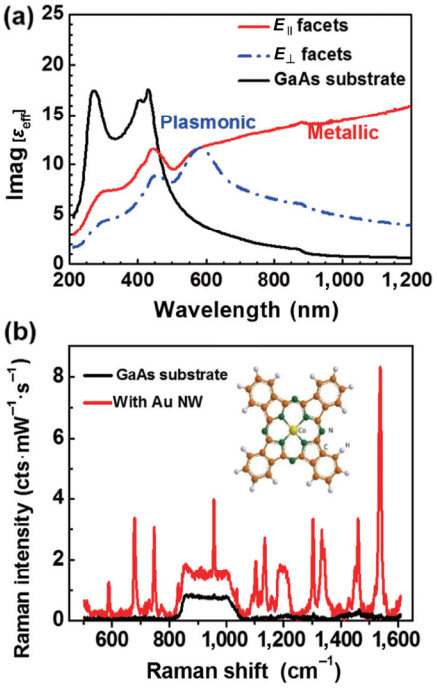

Figure 4 Optical characterization of Au NWs deposited on a periodic, faceted GaAs surface. (a) Polarization-dependent imaginary part of the effective dielectric function measured by spectroscopic ellipsometry. (b) Raman spectra of an ultrathin film (2 nm) of CoPc on bare GaAs and with Au NW, respectively.

for interconnects in nanoelectronics because of their high chemical stability and electrical conductivity. The electrical properties of the fabricated Au nanowire arrays were investigated by KFM, and the *I*–*V* curve of a single Au nanowire is shown in Fig. S5 in the ESM.

Magnetic nanowire arrays are also interesting because of their potential application in high-density magnetic memories or sensors. As an example, in this study, the magnetic properties of the Fe nanowire arrays were investigated by angle-dependent broadband FMR. Figure 5 illustrates the measured in-plane angular dependence of the FMR resonance field of the fabricated Fe nanowire array (Figs. 2(b), 2(d), and 2(f)) at a microwave frequency of 25 GHz. The inset in Fig. 5 reveals the frequency-field dependence along the out-of-plane axis (square), the in-plane long axis (diamond), and the in-plane short axis (circles). A strong increase of the resonance field is observed as the field is rotated from the nanowire long axis (ϕ = 0°, 180°) to the short axis (ϕ = 90°), which is due to the strong shape anisotropy of the nanowires and can be calculated using the wires' demagnetization factor, N_y. The fittings corresponding to the theoretical model (see FMR equation in the ESM) are also illustrated as red solid lines in Fig. 5. With the fitting parameters provided in Table 1, good quantitative agreement between the fitting results and the experimental measurement was obtained. This analysis yielded a vast in-plane shape anisotropy of $\frac{1}{2}\mu_0 N_y M_S^2$ = 583.3 kJ·m^{-3}, where μ_0 is the vacuum permeability and M_S the saturation magnetization. This corresponds to an anisotropy field of $\mu_0 N_y M_S$ = 696 mT originating from the large width-to-height ratio of the wires. However, the counteracting stray fields of neighboring wires reduce the effective in-plane anisotropy to $K_{ip,eff} = \frac{1}{2}\mu_0 N_y M_S^2 - K_{2||}$ = 345.2 kJ·m^{-3}, where $K_{2||}$ is the uniaxial in-plane anisotropy. This corresponds to the effective anisotropy field of $\mu_0 H_{Kip,eff} = \mu_0 N_y M_S - 2K_{2||}/M_S$ = 412 mT. To the best of our knowledge, this is the largest in-plane magnetic anisotropy field obtained by self-assembly techniques [10, 50–53]. Thus, these faceted Fe nanowires can serve as the foundation for in-plane anisotropy optimization, with the possibility of achieving even higher values. The easy large-scale fabrication may be useful for many devices requiring high in-plane anisotropies, such as radio frequency (RF) devices [54]. Moreover, applications as magnetic waveguides [55, 56], wires for domain wall propagation [57, 58], or even biomagnetic sensors [59] are conceivable.

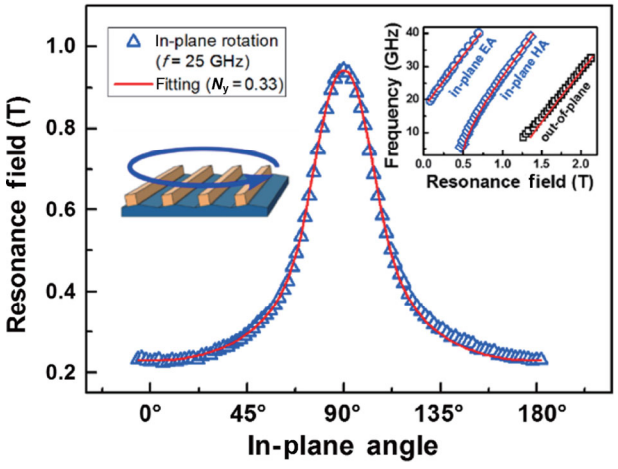

Figure 5 In-plane angle-dependent plot of the resonance field at a microwave frequency of f = 25 GHz. The inset shows the broadband FMR characterization along the three main axes. The red fitting lines reveal significant effective in-plane anisotropy of $K_{ip,eff}$ = 345.2 kJ·m^{-3} ($\mu_0 H_{Kip,eff}$ = 412 mT).

4 Conclusions

In summary, we have demonstrated an efficient method to fabricate diverse metallic nanowires by using a two-step method on periodic and faceted templates obtained by ion irradiation-induced "reverse epitaxy". Because of the extreme regularity and ultrahigh density on a macroscopic length scales, the strong optical anisotropy of the fabricated Au nanowire arrays is promising for application as anisotropic plasmonic SERS sensors. Very large in-plane magnetic

Table 1 Fitting parameters used for the FMR characterization depicted in Fig. 5

Parameter	N_y	g-factor	M_S (kA·m^{-1})	$K_{2\perp}$ (J·m^{-3})[a]	$K_{2||}$ (J·m^{-3})[a]	$K_{4\perp}$ (J·m^{-3})[a]	$K_{4||}$ (J·m^{-3})
Value	0.33	2.09	1,677	0	238.1	67.9	60.4

[a]$K_{2\perp}$ ($K_{2||}$) and $K_{4\perp}$ ($K_{4||}$) are the uniaxial and fourfold out-of-plane (in-plane) anisotropy constants, respectively.

anisotropy was obtained in the prepared Fe nanowire arrays that can serve as a foundation for high magnetic anisotropy tuning and multiple applications, such as, RF devices, magnetic waveguides and even biomagnetic sensors. Moreover, thanks to the crystalline surfaces of the templates, this two-step nanowires fabrication method can be further developed to fabricate other crystalline material nanowires such as semiconductors that can be deposited on the faceted templates. Overall, our finding offers an elegant alternative to large-scale patterning techniques because of its high regularity, and it will inspire further investigations on nanowire-based devices.

Acknowledgements

This work was supported by the National Natural Science Foundation of China (Nos. 11622545 and U1732268), One Hundred Talent Program of CAS and the Deutsche Forschungsgemeinschaft (No. LE2443/5-1). R. D. R. acknowledges the supports from the DFG Unit SMINT FOR1713, Tomsk Polytechnic University Competitiveness Enhancement Program grant, Project Number TPU CEP_IHTP_73\2017, and the EU COST Action MP 1302 Nanospectroscopy.

Electronic Supplementary Material: Supplementary material (morphology of the templates, deposition thickness effects for Au nanowires, fabrication of diverse metallic nanowires, the microstructure of Au and Fe nanowires, and ferromagnetic resonance equation) is available in the online version of this article at https://doi.org/10.1007/s12274-017-1793-y.

References

[1] Xia, Y. N.; Yang, P. D.; Sun, Y. G.; Wu, Y. Y.; Mayers, B.; Gates, B.; Yin, Y. D.; Kim, F.; Yan, Y. Q. One-dimensional nanostructures: Synthesis, characterization, and applications. *Adv. Mater.* **2003**, *15*, 353–389.

[2] Sun, S. H.; Murray, C. B.; Weller, D.; Folks, L.; Moser, A. Monodisperse FePt nanoparticles and ferromagnetic FePt nanocrystal superlattices. *Science* **2000**, *287*, 1989–1992.

[3] Wu, Y.; Xiang, J.; Yang, C.; Lu, W.; Lieber, C. M. Single-crystal metallic nanowires and metal/semiconductor nanowire heterostructures. *Nature* **2004**, *430*, 61–65.

[4] Teperik, T. V.; de Abajo, F. J. G.; Borisov, A. G.; Abdelsalam, M.; Bartlett, P. N.; Sugawara, Y.; Baumberg, J. J. Omnidirectional absorption in nanostructured metal surfaces. *Nat. Photonics* **2008**, *2*, 299–301.

[5] Kawamori, M.; Asai, T.; Shirai, Y.; Yagi, S.; Oishi, M.; Ichitsubo, T.; Matsubara, E. Three-dimensional nanoelectrode by metal nanowire nonwoven clothes. *Nano Lett.* **2014**, *14*, 1932–1937.

[6] Celle, C.; Mayousse, C.; Moreau, E.; Basti, H.; Carella, A.; Simonato, J. P. Highly flexible transparent film heaters based on random networks of silver nanowires. *Nano Res.* **2012**, *5*, 427–433.

[7] Wang, X.; Ozkan, C. S. Multisegment nanowire sensors for the detection of DNA molecules. *Nano Lett.* **2008**, *8*, 398–404.

[8] Ito, T.; Okazaki, S. Pushing the limits of lithography. *Nature* **2000**, *406*, 1027–1031.

[9] Petit, C.; Taleb, A.; Pileni, M. P. Self-organization of magnetic nanosized cobalt particles. *Adv. Mater.* **1998**, *10*, 259–261.

[10] Jung, Y. S.; Lee, J. H.; Lee, J. Y.; Ross, C. A. Fabrication of diverse metallic nanowire arrays based on block copolymer self-assembly. *Nano Lett.* **2010**, *10*, 3722–3726.

[11] Pang, Y. T.; Meng, G. W.; Zhang, L. D.; Qin, Y.; Gao, X. Y.; Zhao, A. W.; Fang, Q. Arrays of ordered Pb nanowires and their optical properties for laminated polarizers. *Adv. Funct. Mater.* **2002**, *12*, 719–722.

[12] Zong, R. L.; Zhou, J.; Li, Q.; Du, B.; Li, B.; Fu, M.; Qi, X. W.; Li, L. T.; Buddhudu, S. Synthesis and optical properties of silver nanowire arrays embedded in anodic alumina membrane. *J. Phy. Chem. B* **2004**, *108*, 16713–16716.

[13] Choi, J.; Oh, S. J.; Ju, H.; Cheon, J. Massive fabrication of free-standing one-dimensional Co/Pt nanostructures and modulation of ferromagnetism via a programmable barcode layer effect. *Nano Lett.* **2005**, *5*, 2179–2183.

[14] Barranco, A.; Borras, A.; Gonzalez-Elipe, A. R.; Palmero, A. Perspectives on oblique angle deposition of thin films: From fundamentals to devices. *Prog. Mater. Sci.* **2016**, *76*, 59–153.

[15] Sugawara, A.; Haga, Y.; Nittono, O. Self-alignment of metallic nanowires in CaF_2-based composite films grown on stepped NaCl substrates. *J. Magn. Magn. Mater.* **1996**, *156*, 151–152.

[16] Teichert, C.; Lagally, M. G.; Peticolas, L. J.; Bean, J. C.; Tersoff, J. Stress-induced self-organization of nanoscale structures in SiGe/Si multilayer films. *Phys. Rev. B* **1996**, *53*, 16334–16337.

[17] Heffelfinger, J. R.; Bench, M. W.; Carter, C. B. On the faceting of ceramic surfaces. *Surf. Sci.* **1995**, *343*, L1161–L1166.

[18] Sugawara, A.; Coyle, T.; Hembree, G. G.; Scheinfein, M. R. Self-organized Fe nanowire arrays prepared by shadow deposition on NaCl(110) templates. *Appl. Phys. Lett.* **1997**, *70*, 1043–1045.

[19] Teichert, C.; Barthel, J.; Oepen, H. P.; Kirschner, J. Fabrication of nanomagnet arrays by shadow deposition on self-organized semiconductor substrates. *Appl. Phys. Lett.* **1999**, *74*, 588–590.

[20] Westphalen, A.; Zabel, H.; Theis-Bröhl, K. Magnetic nanowires on faceted sapphire surfaces. *Thin Solid Films* **2004**, *449*, 207–214.

[21] Facsko, S.; Dekorsy, T.; Koerdt, C.; Trappe, C.; Kurz, H.; Vogt, A.; Hartnagel, H. L. Formation of ordered nanoscale semiconductor dots by ion sputtering. *Science* **1999**, *285*, 1551–1553.

[22] Bradley, R. M.; Harper, J. M. E. Theory of ripple topography induced by ion bombardment. *J. Vac. Sci. Technol. A* **1988**, *6*, 2390–2395.

[23] Norris, S. A. Stress-induced patterns in ion-irradiated silicon: Model based on anisotropic plastic flow. *Phys. Rev. B* **2012**, *86*, 235405.

[24] Carter, G.; Vishnyakov, V. Roughening and ripple instabilities on ion-bombarded Si. *Phys. Rev. B* **1996,** *54*, 17647–17653.

[25] Ziberi, B.; Frost, F.; Höche, T.; Rauschenbach, B. Ripple pattern formation on silicon surfaces by low-energy ion-beam erosion: Experiment and theory. *Phys. Rev. B* **2005**, *72*, 235310.

[26] Mollick, S. A.; Ghose, D.; Shipman, P. D.; Mark Bradley, R. Anomalous patterns and nearly defect-free ripples produced by bombarding silicon and germanium with a beam of gold ions. *Appl. Phys. Lett.* **2014**, *104*, 043103.

[27] Toma, A.; Chiappe, D.; Massabò, D.; Boragno, C.; de Mongeot, F. B. Self-organized metal nanowire arrays with tunable optical anisotropy. *Appl. Phys. Lett.* **2008**, *93*, 163104.

[28] Oates, T. W. H.; Keller, A.; Noda, S.; Facsko, S. Self-organized metallic nanoparticle and nanowire arrays from ion-sputtered silicon templates. *Appl. Phys. Lett.* **2008**, *93*, 063106.

[29] Ranjan, M.; Oates, T. W. H.; Facsko, S.; Möller, W. Optical properties of silver nanowire arrays with 35 nm periodicity. *Opt. Lett.* **2010**, *35*, 2576–2578.

[30] Ou, X.; Kögler, R.; Wei, X.; Mücklich, A.; Wang, X.; Skorupa, W.; Facsko, S. Fabrication of horizontal silicon nanowire arrays on insulator by ion irradiation. *AIP Adv.* **2011**, *1*, 042174.

[31] Ou, X.; Keller, A.; Helm, M.; Fassbender, J.; Facsko, S. Reverse epitaxy of Ge: Ordered and faceted surface patterns. *Phys. Rev. Lett.* **2013**, *111*, 016101.

[32] Ou, X.; Heinig, K. H.; Hübner, R.; Grenzer, J.; Wang, X.; Helm, M.; Fassbender, J.; Facsko, S. Faceted nanostructure arrays with extreme regularity by self-assembly of vacancies. *Nanoscale* **2015**, *7*, 18928–18935.

[33] Chowdhury, D.; Ghose, D. Nanoripple formation on GaAs (001) surface by reverse epitaxy during ion beam sputtering at elevated temperature. *Appl. Surf. Sci.* **2016**, *385*, 410–416.

[34] Zhu, H. J.; Ramsteiner, M.; Kostial, H.; Wassermeier, M.; Schönherr, H. P.; Ploog, K. Room-temperature spin injection from Fe into GaAs. *Phys. Rev. Lett.* **2001**, *87*, 016601.

[35] Chantis, A. N.; Belashchenko, K. D.; Smith, D. L.; Tsymbal, E. Y.; van Schilfgaarde, M.; Albers, R. C. Reversal of spin polarization in Fe/GaAs (001) driven by resonant surface states: First-principles calculations. *Phys. Rev. Lett.* **2007**, *99*, 196603.

[36] Pierre-Louis, O.; D'Orsogna, M. R.; Einstein, T. L. Edge diffusion during growth: The kink Ehrlich–Schwoebel effect and resulting instabilities. *Phys. Rev. Lett.* **1999**, *82*, 3661–3664.

[37] Kneedler, E. M.; Jonker, B. T.; Thibado, P. M.; Wagner, R. J.; Shanabrook, B. V.; Whitman, L. J. Influence of substrate surface reconstruction on the growth and magnetic properties of fe on GaAs(001). *Phys. Rev. B* **1997**, *56*, 8163–8168.

[38] Schönherr, H.-P.; Nötzel, R.; Ma, W. Q.; Ploog, K. H. Evolution of the surface morphology of Fe grown on GaAs (100), (311)A, and (331)A substrates by molecular beam epitaxy. *J. Appl. Phys.* **2001**, *89*, 169–173.

[39] Hong, S. W.; Huh, J.; Gu, X. D.; Lee, D. H.; Jo, W. H.; Park, S.; Xu, T.; Russell, T. P. Unidirectionally aligned line patterns driven by entropic effects on faceted surfaces. *Proc. Natl. Acad. Sci. USA* **2012**, *109*, 1402–1406.

[40] Hong, S. W.; Voronov, D. L.; Lee, D. H.; Hexemer, A.; Padmore, H. A.; Xu, T.; Russell, T. P. Controlled orientation of block copolymers on defect-free faceted surfaces. *Adv. Mater.* **2012**, *24*, 4278–4283.

[41] Biermanns, A.; Pietsch, U.; Grenzer, J.; Hanisch, A.; Facsko, S.; Carbone, G.; Metzger, T. H. X-ray scattering and diffraction from ion beam induced ripples in crystalline silicon. *J. Appl. Phys.* **2008**, *104*, 044312.

[42] Garel, M.; Babonneau, D.; Boulle, A.; Pailloux, F.; Coati, A.; Garreau, Y.; Ramos, A. Y.; Tolentino, H. C. N. Self-organized ultrathin FePt nanowires produced by glancing-angle ion-beam codeposition on rippled alumina surfaces. *Nanoscale* **2015**, *7*, 1437–1445.

[43] Linic, S.; Aslam, U.; Boerigter, C.; Morabito, M. Photochemical transformations on plasmonic metal nanoparticles. *Nat. Mater.* **2015**, *14*, 567–576.

[44] Au, L.; Chen, Y.; Zhou, F.; Camargo, P. H. C.; Lim, B.; Li, Z. Y.; Ginger, D. S.; Xia, Y. N. Synthesis and optical properties of cubic gold nanoframes. *Nano Res.* **2008**, *1*, 441–449.

[45] Nie, S. M.; Emory, S. R. Probing single molecules and single nanoparticles by surface-enhanced Raman scattering. *Science* **1997**, *275*, 1102–1106.

[46] Kneipp, K.; Wang, Y.; Kneipp, H.; Perelman, L. T.; Itzkan, I.; Dasari, R. R.; Feld, M. S. Single molecule detection using surface-enhanced Raman scattering (SERS). *Phys. Rev. Lett.* **1997**, *78*, 1667–1670.

[47] Zhou, Q.; Yang, Y.; Ni, J.; Li, Z. C.; Zhang, Z. J. Rapid recognition of isomers of monochlorobiphenyls at trace levels by surface-enhanced Raman scattering using ag nanorods as a substrate. *Nano Res.* **2010**, *3*, 423–428.

[48] Johnson, P. B.; Christy, R.-W. Optical constants of the noble metals. *Phys. Rev. B* **1972**, *6*, 4370–4379.

[49] Sheremet, E.; Rodriguez, R. D.; Zahn, D. R. T.; Milekhin, A. G.; Rodyakina, E. E.; Latyshev, A. V. Surface-enhanced Raman scattering and gap-mode tip-enhanced Raman scattering investigations of phthalocyanine molecules on gold nanostructured substrates. *J. Vac. Sci. Technol. B* **2014**, *32*, 04E110.

[50] Qin, D. H.; Cao, L.; Sun, Q. Y.; Huang, Y.; Li, H. L. Fine magnetic properties obtained in FeCo alloy nanowire arrays. *Chem. Phys. Lett.* **2002**, *358*, 484–488.

[51] Wang, J.; Chen, Q.; Zeng, C.; Hou, B. Magnetic-field-induced growth of single-crystalline Fe_3O_4 nanowires. *Adv. Mater.* **2004**, *16*, 137–140.

[52] Chaure, N. B.; Stamenov, P.; Rhen, F. M. F.; Coey, J. M. D. Oriented cobalt nanowires prepared by electrodeposition in a porous membrane. *J. Magn. Magn. Mater.* **2005**, *290–291*, 1210–1213.

[53] Maurer, T.; Ott, F.; Chaboussant, G.; Soumare, Y.; Piquemal, J. Y.; Viau, G. Magnetic nanowires as permanent magnet materials. *Appl. Phys. Lett.* **2007**, *91*, 172501.

[54] Tseng, A. A.; Shirakashi, J.-I.; Nishimura, S.; Miyashita, K.; Notargiacomo, A. Scratching properties of nickel-iron thin film and silicon using atomic force microscopy. *J. Appl. Phys.* **2009**, *106*, 044314.

[55] Topp, J.; Heitmann, D.; Kostylev, M. P.; Grundler, D. Making a reconfigurable artificial crystal by ordering bistable magnetic nanowires. *Phys. Rev. Lett.* **2010**, *104*, 207205.

[56] Körner, M.; Lenz, K.; Gallardo, R. A.; Fritzsche, M.; Mücklich, A.; Facsko, S.; Lindner, J.; Landeros, P.; Fassbender, J. Two-magnon scattering in permalloy thin films due to rippled substrates. *Phys. Rev. B* **2013**, *88*, 054405.

[57] Hayashi, M.; Thomas, L.; Rettner, C.; Moriya, R.; Parkin, S. S. P. Direct observation of the coherent precession of magnetic domain walls propagating along permalloy nanowires. *Nat. Phys.* **2007**, *3*, 21–25.

[58] Allwood, D. A.; Xiong, G.; Faulkner, C. C.; Atkinson, D.; Petit, D.; Cowburn, R. Magnetic domain-wall logic. *Science* **2005**, *309*, 1688–1692.

[59] Huang, H. T.; Ger, T. R.; Lin, Y. H.; Wei, Z. H. Single cell detection using a magnetic zigzag nanowire biosensor. *Lab Chip* **2013**, *13*, 3098–3104.